Journal of Molecular Structure 519 (2000) 101–117

Journal of
MOLECULAR
STRUCTURE

www.elsevier.nl/locate/molstruc

# The vibrational spectra including matrix isolation, conformations and ab initio calculations of 4-azidobut-1-yne

A. Gatial[a,*], S. Sklenák[a,1], P. Klaeboe[b], C.J. Nielsen[b], H. Priebe[b], R. Salzer[b,2], D. Kurková[b]

[a]*Department of Physical Chemistry, Slovak Technical University, 81237 Bratislava, Slovak Republic*
[b]*Department of Chemistry, University of Oslo, P.O. Box 1033 Blindern, 0315 Oslo 3, Norway*

Received 20 April 1999; accepted 18 May 1999

## Abstract

4-Azidobut-1-yne can exist in five distinct conformations denoted GG, GG′, GA, AG and AA according to the *gauche* and *anti* conformation around C–C and the C–N bonds, respectively. Fully optimised ab initio geometries for all five conformers have been calculated at the MP2(full)/TZ2P//MP2(full)/TZ2P level. The calculated conformational energies were GG (0), AG (+1.24 kJ mol$^{-1}$), AA (+1.50 kJ mol$^{-1}$), GG′ (+3.35 kJ mol$^{-1}$) and GA (+3.75 kJ mol$^{-1}$). Additional single point calculations were also performed at the MP4(DSQ)/TZ2P//MP2(full)/TZ2P level for all five conformers.

IR spectra of the molecule were obtained in the vapour and liquid states at room temperature and as amorphous and crystalline solids at liquid nitrogen temperature. Additional IR spectra of argon and nitrogen matrices were recorded, applying the hot nozzle technique with temperatures between 313 and 600 K. Raman spectra of the liquid in the temperature range 232–295 K and of a crystalline solid at 148 K were also measured.

A number of strong bands disappeared in the crystal phase. The same bands increased their relative intensity upon annealing of the low temperature matrices suggesting that the most stable conformer in the vapour and in the liquid is not the one present in the crystal phase. Apparently, all five conformers are present in the liquid at room temperature and in the argon matrix at 12 K, whereas only three conformers (GG, AG and AA) were observed in the nitrogen matrix. The liquid phase Raman spectra and the hot nozzle IR matrix isolation spectra showed very small temperature variations and it was not possible to estimate the energy differences between conformers.

To assist in the spectral assignment, the ab initio force fields for all conformers were scaled using six scale factors. The results suggest that the conformer present in the crystal phase is AG and the most stable conformer in the liquid as well as in the low temperature matrices is GG.

*Keywords:* Conformations; Azides; Infrared spectroscopy; Raman spectroscopy; Ab initio calculations

## 1. Introduction

In 4-azidobut-1-yne ($HC{\equiv}C{-}CH_2{-}CH_2{-}N_3$, later to be abbreviated BUTAZ) there are conformational minima due to restricted rotations around the C–C bond (*gauche* or *anti*) and around the C–N bond (*gauche* or *anti*). Therefore, BUTAZ can exist in

---

[*] Corresponding author. Tel.: +421-7-52926032; fax: +421-7-52493198.

*E-mail address:* gatial@cvt.stuba.sk (A. Gatial).

[1] Permanent address: Chemical Faculty, Technical University Brno, 63700 Brno, Czech Republic.

[2] Permanent address: Department of Analytical Chemistry, Technical University Dresden, 01062 Dresden, Germany.

PII: S0022-2860(99)00282-3

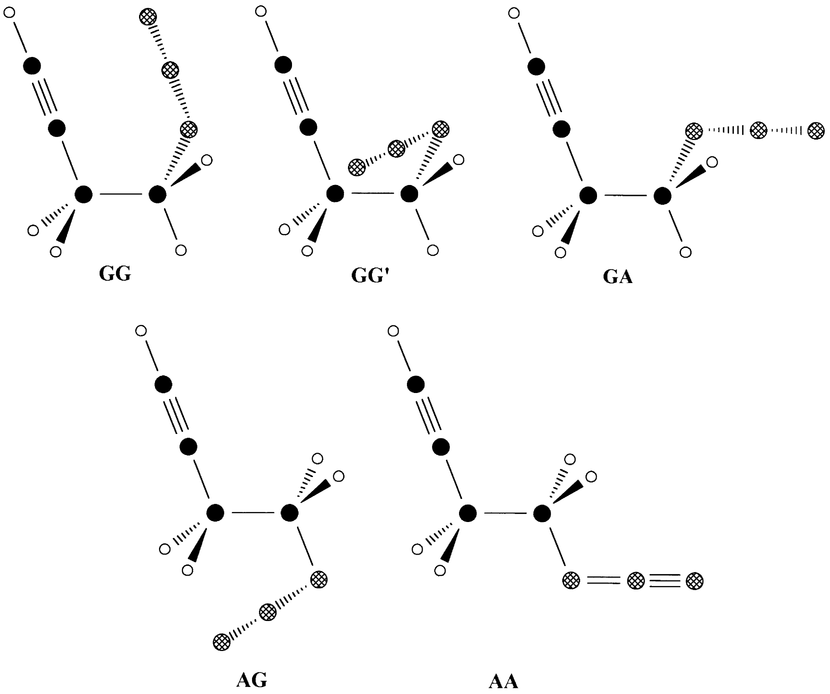

Fig. 1. The five possible conformations of 4-azidobut-1-yne (BUTAZ). GG: $\tau_{C\text{–}C} = -60$, $\tau_{C\text{–}N} = 60$; GG′: $\tau_{C\text{–}C} = -60$, $\tau_{C\text{–}N} = -60$; GA: $\tau_{C\text{–}C} = -60$, $\tau_{C\text{–}N} = 180$; AG: $\tau_{C\text{–}C} = 180$, $\tau_{C\text{–}N} = 60$; AA: $\tau_{C\text{–}C} = 180$, $\tau_{C\text{–}N} = 180$.

five distinct conformations, shown in Fig. 1 and labelled by GG, GG′, GA, AG and AA, where the letters indicate the conformation around the C–C and the C–N bonds, respectively.

We have previously studied several organic azides with a $-CH_2N_3$ moiety by electron diffraction, vibrational spectroscopy and by ab initio methods, i.e. 3-azidopropene ($CH_2{=}CH{-}CH_2N_3$) [1,2], azidoacetonitrile ($N{\equiv}C{-}CH_2N_3$) [3], 3-azidopropyne (propargylazide $HC{\equiv}C{-}CH_2N_3$) [4], azidobut-2-yne ($CH_3C{\equiv}C{-}CH_2N_3$) [5], and azidoethane ($CH_3{-}CH_2N_3$) [6].

The previous experimental results for the acetylenic azides [3–5] showed unambiguously that these compounds exist only in the *gauche* conformation and established the stabilising effect of orienting the azido group towards the π-electron system of the acetylenic bond. The same results were obtained in a recent high level ab initio study of small organic azides [7] where the *anti* orientation of the azido group was calculated to give 5.6, 7.2 and 7.8 kJ mol$^{-1}$ higher energy for azidoacetonitrile, 3-azidopropyne and azidobut-2-yne, respectively. Also in 3-azidopropene, with five possible conformations, the two conformers with the azido group oriented towards the vinyl group (GG, SG) were found as the more stable. In azidoethane there are conformational possibilities around the C–N bond but here the stabilising effects are absent. Accordingly, the experimental results revealed that the energy difference between the *gauche* and *anti* orientation is very low with the *gauche* conformer being only 0.6 kJ mol$^{-1}$ more stable than *anti* in the vapour phase [6].

In the previously studied unsaturated organic azides, the $-CH_2N_3$ moiety was adjacent to the π-bond system. In BUTAZ, however, an additional methylene group separates the azido group is from the π-bond system (Fig. 1) and a smaller conformational stabilisation is therefore expected. Preliminary experimental and theoretical results for BUTAZ [8,9] were in part inconsistent. The results of more rigorous ab initio calculations together with a complete interpretation of the vibrational spectra are given in the present paper.

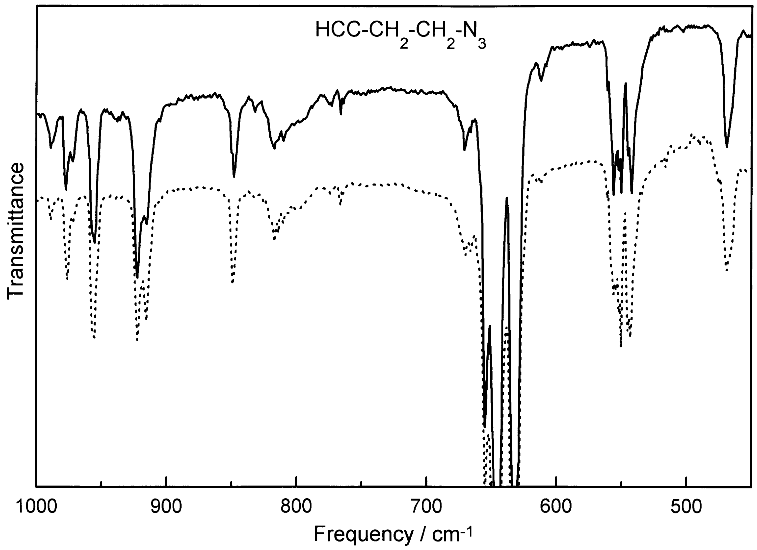

Fig. 2. Infrared spectra of BUTAZ in Ar matrix deposited with the nozzle temperature 313 K (solid line) and after 30 min annealing at 34 K (dotted line).

## 2. Experimental

The sample was synthesised by the method described previously [10]. IR spectra of the vapour, liquid, solid and the inert matrices were recorded with a Bruker model 88 Fourier transform spectrometer and a Perkin–Elmer model 225 spectrometer in the middle IR (MIR) and a Bruker model 114c in the far IR region (FIR). The vapour spectra were recorded in cells with 10 and 1 m path lengths. A simple glass cryostat cooled with liquid nitrogen was applied for the solid, and a closed-cycle He-cooled cryostat from Air Products was used for the matrix spectra. The matrix spectra were obtained with both nitrogen and argon as matrix materials and with matrix/sample ratios of 1:300 and 1:500. The gas mixtures were passed through an electrically heated quartz nozzle [11] before being deposited on the cold CsI window kept at 12–14 K. No pyrolysis products were detected employing nozzle temperatures of 313, 450 and 600 K for the nitrogen and 313 and 600 K for the argon experiments. The argon matrices were annealed between 30 min and 14 h at 34 K, and 2 h at 38 K. The nitrogen matrices were annealed for 1 h at temperatures in the range 27–34 K and ultimately for 12 h at 29 K and 2 h at 32 K.

Raman spectra were recorded on a DILOR RTI 30 spectrometer (triple monochromator) interfaced to the Aspect 2000 data system of the Bruker FTIR. The 514.8 nm line of a Spectra Physics model 2000 Ar ion laser was used for excitation. The liquid spectra were recorded at various temperatures in the range 232–295 K in an ampoule inserted in a Dewar [12] and cooled with gaseous nitrogen evaporating from a reservoir equipped with a heating element. The sample turned crystalline instantaneously below 200 K and crystal spectra were measured of the same ampoule at 148 and 178 K.

## 3. Results and discussion

The spectral data are collected in Table 1. From the numerous spectra of BUTAZ we have selected a few illustrative examples. Fig. 2 shows part of the infrared spectrum (1000–450 $cm^{-1}$) of BUTAZ isolated in argon at 12 K and obtained with a nozzle temperature of 313 K. Fig. 2 also includes the spectrum recorded after annealing to 34 K. Spectra of argon and nitrogen matrices in the same region, obtained with a nozzle temperature of 600 K, are given in Fig. 3. The infrared spectrum of the liquid at room temperature in the region 1500–450 $cm^{-1}$ is reproduced in Fig. 4; the spectra of the amorphous and crystalline solids at

Table 1
Infrared and Raman spectral data for 4-azidobut-1-yne (weak bands in the regions 4000–3400, 2800–2300 and 2000–1600 cm$^{-1}$ have been omitted)

| Infrared | | | | | | Raman | | Interpretation[a] |
|---|---|---|---|---|---|---|---|---|
| Vapour 295 K | N$_2$ matrix 600 K[b] | Ar matrix 600 K | Liquid 295 K | Amorphous solid 80 K | Crystalline solid 80 K | Liquid 295 K | Crystalline solid 148 K | |
| 3334 s[c] | | 3326 s | | | 3294 s | | | |
| | | 3322 s | 3313 s | 3282 s | 3280 vs | 3301 w | 3285 w | $\nu_1$ |
| 3325 s | | | | | | | | |
| 3315 mw,sh | 3298 w | 3300 w,sh | 3294 m | 3260 m,sh | 3266 vw | 3290 vw,sh | | |
| 3305 w,sh | | | | | | | | |
| 2998 w,sh | | | | | 2996 vw | | 2995 w | |
| 2988 m,w | 2988 w | 2983 w | 2978 w | 2980 vw,brd | 2987 w | 2987 m | | $\nu_2$ |
| 2960 m | 2959 m | 2956 w | | | | | | |
| 2952 m | 2948 m | 2944 m | 2940 m | 2946 mw | 2951 m | 2940 s,sh | 2948 w | $\nu_3$ |
| 2938 m | 2938 w,sh | 2938 w | | 2936 w,sh | 2933 w | | 2936 m | $\nu_4$ |
| 2929 m | 2930 w | 2932 w | | | | | | |
| 2921 w | 2920 w,sh | 2918 w | 2920 w | 2915 w | 2913 w | 2920 vs | 2917 s | $\nu_5$ |
| 2887 mw | | | | | 2891 vw | | 2894 w | |
| 2882 mw | 2884 mw | 2881 mw | 2879 m | 2883 w,sh | 2881 w | 2882 m | 2885 vvw | |
| 2876 mw | | 2874 w,sh | | 2876 w | | | | |
| 2863 vw | 2858 vw | | 2850 vw,sh | | 2840 vw | 2849 w | 2840 vw | |
| | | | | | | 2835 vw | | |
| 2196 m | 2188 m | 2191 m | 2180 m,sh | 2181 mw | 2179 mw | | | |
| | 2180 m | 2179 w,sh | | | | | | |
| | 2160 m | 2161 w,sh | | | 2162 m | | | |
| 2166 m | 2150 m | 2152 m | 2155 m | 2156 m | 2156 m,sh | | | |
| | 2135 s,sh | 2140 m,sh * | | | | | | |
| 2134 s | 2131 s | 2135 s | 2126 s | 2125 vs | 2118 vs | 2122 vvs | 2118 vvs | $\nu_6$ |
| 2114 vs | | | | | 2097 s,sh | | | |
| 2106 vs | 2110 vs | 2106 vs | 2094 vs | 2094 vs | 2091 vs | 2090 m,sh | 2091 m | $\nu_7$ |
| 2100 vs | | 2099 s,sh | | | | | | |
| | 2095 s | 2093 s | | | | | | |
| | 2088 m,sh * | 2082 m,sh * | | 2077 m,sh | 2074 vw | | | |
| 2078 m | 2074 m | 2072 m | 2060 m,sh | 2060 w,sh | 2060 w | 2075 w,sh | 2073 vw | |
| | 2036 vw * | 2042 vw * | | 2031 vw | 2035 vw | | | |
| 1468 mw | | | | 1465 w,sh | 1465 w,sh | | | |
| 1460 mw | 1466 w ⇓ | 1465 vw ⇓ | 1459 m | | | 1461 vw,sh | | $\nu_8$(AG) |
| 1456 mw | 1463 m | 1463 m | 1454 m | 1458 mw | 1461 m | 1456 w | 1459 w | $\nu_8$(GG) |
| 1447 mw | 1460 w | 1458 w | | 1454 mw | 1456 m | | | |
| 1440 w | 1456 vw | 1454 vw | | 1448 w,sh | 1450 w | | | |
| 1436 w | 1439 vw ⇓ | 1436 w ⇓ | 1431 w,sh | 1430 w,sh | 1432 mw | 1433 w,sh | 1430 mw | $\nu_9$(AG) |
| 1432 w | 1431 m | 1429 mw | 1425 m | 1423 mw | * | 1427 m | * | $\nu_9$(GG) |
| 1429 w | 1428 w,sh | | | | | | | |
| 1423 vw | | 1423 vvw | 1419 vw | 1419 w | * | | | |

Table 1 (*continued*)

| Infrared | | | | | | Raman | | Interpretation[a] |
|---|---|---|---|---|---|---|---|---|
| Vapour 295 K | $N_2$ matrix 600 K[b] | Ar matrix 600 K | Liquid 295 K | Amorphous solid 80 K | Crystalline solid 80 K | Liquid 295 K | Crystalline solid 148 K | |
| 1381 vvw | 1382 μ vvw | 1378 vvw | 1380 vvw | 1383 vw | 1383 vvw | | | |
| | | 1364 w,sh | | | | | | |
| 1359 m | 1363 s ⇓ | 1361 s ⇓ | 1356 m | 1363 mw | 1364 w | 1359 vw | 1367 w | $\nu_{10}$(GG,AG) |
| | 1361 w,sh5 | | | | 1361 w,sh | | 1362 w | $2\nu_{20}$ |
| 1352 m | 1353 m+ ↓ ⇓ | 1352 m+ ↓ ⇓ | 1350 m | 1351 m | | 1349 vvw | | $\nu_{10}$(AA) |
| | 1348 vvw? | 1350 w,sh | | | 1346 w | | 1344 vvw | $2\nu_{21}$ |
| 1347 m | | 1344 w * | | 1348 m | | | | $\nu_{10}$(GG$'$,GA) |
| | 1342 vw,sh | 1338 w,sh * | | | | | | |
| 1337 mw | 1337 s+ ↑ ⇑ | 1336 s+ ↑ ⇑ | 1332 m | 1332 m | * | 1334 m | * | $\nu_{11}$(GG,GG$'$,GA) |
| 1330 w | | 1322 m * | | | | | | |
| 1311 mw | 1315 m ⇓ | 1316 mw ⇓ | 1302 w,sh? | 1310 w,sh | 1302 s | | 1309 mw | $\nu_{11}$(AG) |
| | | 1312 m+ * | | | | | | $\nu_{12}$(AA) |
| | | 1309 w+ * | | | | | | $\nu_{12}$(GG$'$,GA) |
| 1294 s | 1298 s ↑ | 1301 s ↑ | 1295 s | 1298 vs | * | 1295 m | * | $\nu_{12}$(GG) |
| | | 1295 w,sh | | | | | | |
| | 1287 m ↓ ⇓ | 1292 s ↓ ⇓ | 1287 w,sh? | 1287 w,sh | * | 1290 w,sh | * | $\nu_{11}$(AA) |
| 1279 s | 1277 s ⇓ | 1276 s ⇓ | | | 1281 w | 1280 m+ | 1279 w | $\nu_{12}$(AG) |
| | | 1272 w,sh * | | | 1275 vw | | | |
| 1271 vs | 1268 vs ⇓ | 1269 vs ⇓ | 1267 s | 1271 s | 1253 s | 1269 w,sh+ | 1256 mw | $\nu_{13}$(AG) |
| 1260 s | 1263 s ⇓ | 1266 s ⇓ | | | 1245 s | | 1250 mw | |
| | | 1263 s ⇓ | | | | | | |
| | | 1259 s ⇓ | | 1265 w,sh | * | | | |
| 1250 m | | 1255 m * | | | | | | $\nu_{13}$(GG$'$,GA)? |
| | | 1252 m * | | | | | | |
| 1239 m | 1245 m ↓ ⇓ | 1243 m ↓ ⇓ | 1242 ms | 1243 mw | * | 1241 mw+ | * | $\nu_{13}$(AA) |
| | 1229 m,sh | 1229 w,sh | | | | | | |
| 1224 mw | 1226 s ↑ | 1226 s ↑ | 1225 m | 1225 mw | * | 1227 m | * | $\nu_{13}$(GG) |
| 1219 w | | 1223 m,sh | | | | | | |
| | 1211 vw ⇓ | 1211 vw | 1206 w | 1210 vw,sh | 1202 m | 1206 w,sh? | 1202 m | $\nu_{14}$(AG) |
| 1203 w | 1206 vw | 1198 vw | 1196 w | 1202 w | | 1199 mw | | $\nu_{14}$(GG) |
| 1192 vw | 1184 w | 1181 w | 1184 vw,sh | 1194 vw,sh | | | | $\nu_{14}$(AA) |
| 1174 vw | | | | 1172 vvw | 1172 vvw | | | |
| 1143 vvw | | | 1152 vw | 1155 vw | 1156 vw | | | |
| | 1105 vvw | 1097 vvw | 1115 w | 1107 vw | 1117 w | 1106 vvw | | |
| | | | 1075 vvw | | | | | |
| 1060 vw | 1058 w ⇓ | 1062 w ⇓ | | | 1058 mw | 1055 w,sh? | 1060 vvw | $\nu_{15}$(AG) |
| 1053 vw | 1055 vw,sh ↑ | 1059 vw,sh ↑ | 1052 w | 1056 w | | 1050 mw | * | $\nu_{15}$(GG) |
| 1043 vvw | 1041 vw ↓ ⇓ | 1040 vvw ↓ ⇓ | | 1041 vw | * | | | $\nu_{15}$(AA), $\nu_{16}$(AA) |
| 1021 vw | 1020 w,sh ⇓ | 1022 vw ⇓ | 1021 vw,sh? | | 1023 m | 1022 w,sh? | 1025 s | $\nu_{16}$(AG) |
| 1016 vw | 1017 w | 1018 w ↑ | 1015 w | 1018 w | | 1018 m | * | $\nu_{16}$(GG) |

Table 1 (*continued*)

| Infrared | | | | | | Raman | | Interpretation[a] |
|---|---|---|---|---|---|---|---|---|
| Vapour 295 K | $N_2$ matrix 600 K[b] | Ar matrix 600 K | Liquid 295 K | Amorphous solid 80 K | Crystalline solid 80 K | Liquid 295 K | Crystalline solid 148 K | |
| 1009 vw | | 1013 vw | | 1010 vw,sh | 1009 vvw | | | |
| | 985 vw ↓ ⇓ | 989 vw ↓ ⇓ | 978 w | 983 w | * | 977 w,sh+ | * | $\nu_{17}$(AA) |
| | | 972 vw,sh ↓ * | | 973 vw,sh | * | 968 vw,sh+ | * | $\nu_{17}$(GG′,GA) |
| 970 w | | | | | | | | |
| 966 w | 974 w ⇓ | 977 w ⇓ | | 956 m,sh | 959 w | 964 m+ | 960 m | $\nu_{17}$(AG) |
| | | | | | 944 w | | 945 m | |
| 956 m | 954 m ↑ | 956 m ↑ | 951 m | 949 s | * | 951 m | * | $\nu_{17}$(GG) |
| 948 m | 941 vw | 939 vvw | | | | | | |
| 919 ms | 919 m ⇓ | 922 m ⇓ | 910 m | 918 m,sh | 908 s | 910 m | 908 s | $\nu_{18}$(AG) |
| | | | | | 896 w,sh | | | |
| 914 ms | 914 mw,sh ↓ ⇓ | 915 mw,sh ↓ ⇓ | | 910 s | * | 906 w,sh | * | $\nu_{18}$(AA) |
| 854 w | | | | | | | | |
| 842 w | 850 mw | 849 w ↑ | 840 w | 843 w | * | 837 w,sh | * | $\nu_{18}$(GG) |
| 833 w | | 832 vvw * | | | | | | $\nu_{18}$(GG′,GA) |
| 821 w | | 817 vw * | 820 mw | 820 mw | * | 822 m,sh | * | $\nu_{19}$(GG′,GA) |
| 812 w | 811 mw | 810 vvw ↑ | 810 w,sh | 810 w,sh | * | 814 ms | * | $\nu_{19}$(GG) |
| 768 vw | 774 vw | 774 vvw ⇓ | 773 vw | 774 w | 773 m | 773 vvw | 775 w | $\nu_{19}$(AG) |
| | | 766 vvw ⇓ | 760 vvw | 750 vvw | * | | | |
| | | | | | 684 vs | | 681 w | $\nu_{20}$(AG) |
| 670 ms,sh | 672 mw | 672 mw | 675 m | 670 vs | 673 vs | 666 w,sh | 672 m | $\nu_{21}$(AG) |
| | | | | | 662 vs | | 662 w | $\nu_{22}$(AG) |
| | | | | | 656 s | | 654 vvw,sh | |
| | 663 s | | | | | | | |
| 653 vs | 658 vs | 656 m | 657 s,sh | 655 vs,brd | * | 654 m | * | $\nu_{20}$(GG) |
| | 655 s | | | | | | | |
| 642 vs | 650 vs | 648 vs | 644 vs,brd | 644 vs,sh | * | 641 m | * | $\nu_{21}$(GG) |
| | 647 s | 645 s,sh | | | | | | |
| 635 vs | 641 vs | 634 vs | 632 s,sh | 630 s,sh | * | 631 m | * | $\nu_{22}$(GG) |
| | | 632 vs | | | | | | |
| | | 630 s | | | | | | |
| 568 m | | 561 w | | | | | | |
| 556 m | 557 m | 556 mw | 554 mw | 556 s | 558 s | 556 vvw | 557 vvw | $\nu_{23}$(GG,AG) |
| 550 m | 552 m | 550 m | | | | | | |
| 545 s | 545 m | 545 m | | | | | | |
| 539 s | 542 m | 543 m | 541 m | 543 s | * | 542 w | * | $\nu_{24}$(GG) |
| 533 s | | | | | | | | |
| 476 m | | | | | | | | |
| 467 m | 470 m ⇓ | 470 mw ⇓ | 473 mw | 476 m | 475 s | 476 m+ | 476 ms | $\nu_{24}$(AG) |
| 456 m | | | | | | | | |
| 383 w | | | | | | | | |

Table 1 (*continued*)

| Infrared | | | | | | Raman | | Interpretation[a] |
|---|---|---|---|---|---|---|---|---|
| Vapour 295 K | $N_2$ matrix 600 K[b] | Ar matrix 600 K | Liquid 295 K | Amorphous solid 80 K | Crystalline solid 80 K | Liquid 295 K | Crystalline solid 148 K | |
| 374 w | 374 vw | 372 vvw | | 374 w | 374 s,sh | 369 w,sh | 371 m | $\nu_{25}$(GG,AG) |
| 362 w | 361 vw | | | | 369 s | | | |
| | 355 vw | 355 vw | | | | | | |
| 350 m | 347 m | 348 m | | 355 m,sh | 350 s | 349 m,sh+ | 349 vs | $\nu_{26}$(AG) |
| 340 m | 340 m | 339 m | | 344 s | * | 332 s | * | $\nu_{26}$(GG) |
| 334 m | | | | | | | | |
| 327 m,sh | 335 m+ | 334 m+ | | 335 w,sh | * | | * | $\nu_{26}$(AA)? |
| 323 m,sh | | | | | | | | |
| 260 m | | | | | | | | |
| 253 m | 264 w,sh | 264 w | | 264 m | * | 260 m | * | $\nu_{27}$(GG) |
| 246 m | 260 mw | 258 mw | | 247 w,sh | 255 m | 252 w,sh+ | 247 ms | $\nu_{27}$(AG) |
| | | | | | 247 vw,sh | | | |
| | | | | | | 178 s | 195 s | $\nu_{28}$(AG) |
| | | | | | | 165 ? | | |
| | | | | | | | 94 vvs | $\nu_{29}$(AG) |
| | | | | | | | 40 m | $\nu_{30}$(AG) |

[a] For the description of the vibrations, cf. Tables 4 and 5.

[b] Temperature of the gas before deposition upon the cold window.

[c] Abbreviations: s, strong; m, medium; w, weak; v, very; sh, shoulder; brd, broad; + denotes bands which increase in relative intensity with increasing of the (nozzle) temperature; ↓ and ↑ denote bands which decrease or increase in relative intensity upon the mild annealing, ⇓ and ⇑ denote bands which decrease or increase in relative intensity upon the intensive annealing; * denotes bands which disappear after annealing of the matrix or vanishing in the solid phase.

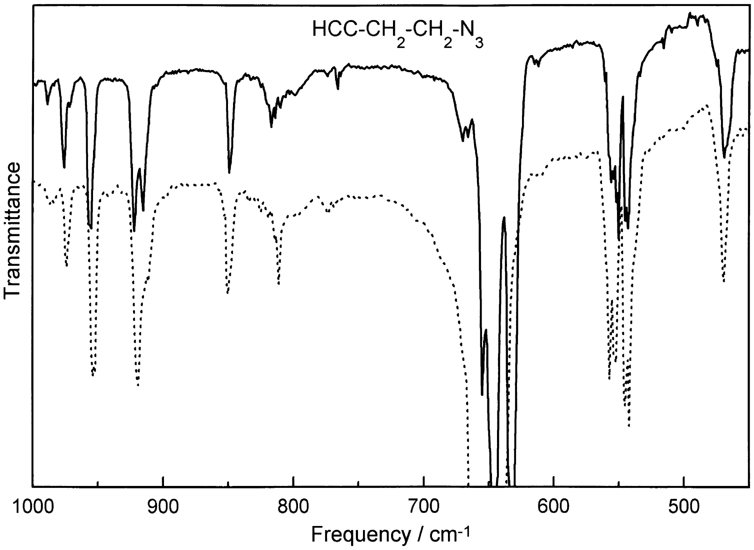

Fig. 3. Infrared spectra of BUTAZ in Ar matrix (solid line) and in $N_2$ matrix (dotted line) deposited with the nozzle temperature 600 K.

80 K in the same region are shown in Figs. 5 and 6, respectively. The Raman spectra of the liquid at 295 K and of the crystalline solid at 148 K are given in Fig. 7, and a comparison between the Raman spectra of the liquid at 232 and 293 K is presented in Fig. 8.

### 3.1. Spectra of the liquid and amorphous solid

Of the 30 vibrational fundamentals 23 are expected to fall below 1500 cm$^{-1}$. A simple count of the infrared and Raman bands in the liquid and

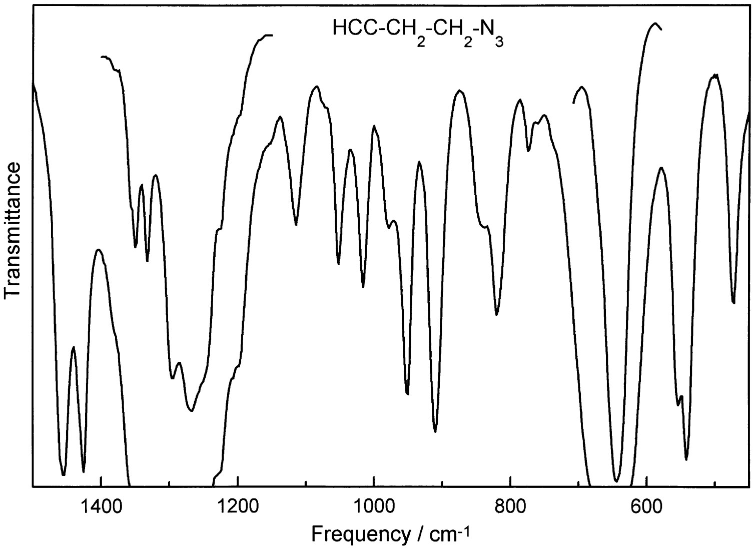

Fig. 4. Infrared spectrum of BUTAZ as a liquid at 295 K.

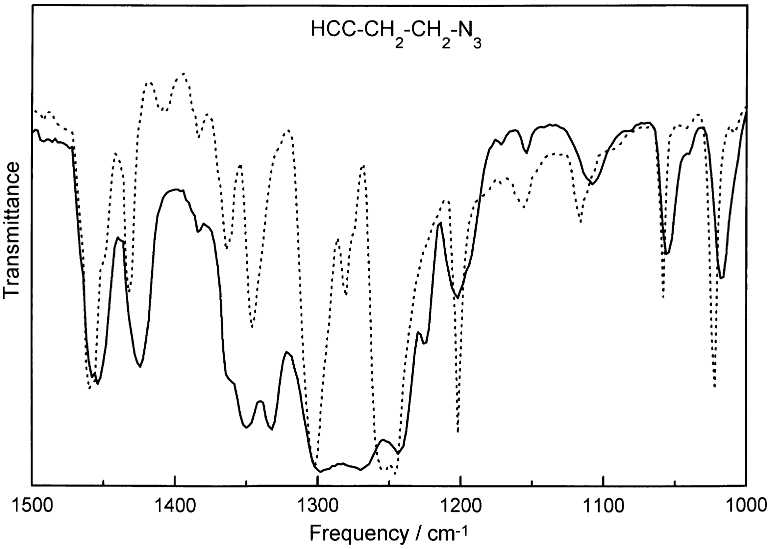

Fig. 5. Infrared spectrum of BUTAZ as an amorphous solid (solid line) and as a crystalline solid (dotted line) at 80 K in the region 1500–1000 cm$^{-1}$.

amorphous solid spectra (Figs. 4, 5, 6 and 8) reveals additional strong bands, indicating that the compound exists in at least two, and probably even more conformers. The Raman spectra of the liquid, recorded at 232 and 293 K, show only minute intensity changes as presented in Fig. 8. This suggests very small energy differences between the main BUTAZ conformers. This conclusion is also supported by the similarity between the infrared spectra of the liquid and amorphous solid (assuming that the barriers between the BUTAZ conformers are relatively low, similar to the situation in 3-azidopropene [1,2]).

Various attempts were made to extract information on the conformational equilibria by curve analyses of

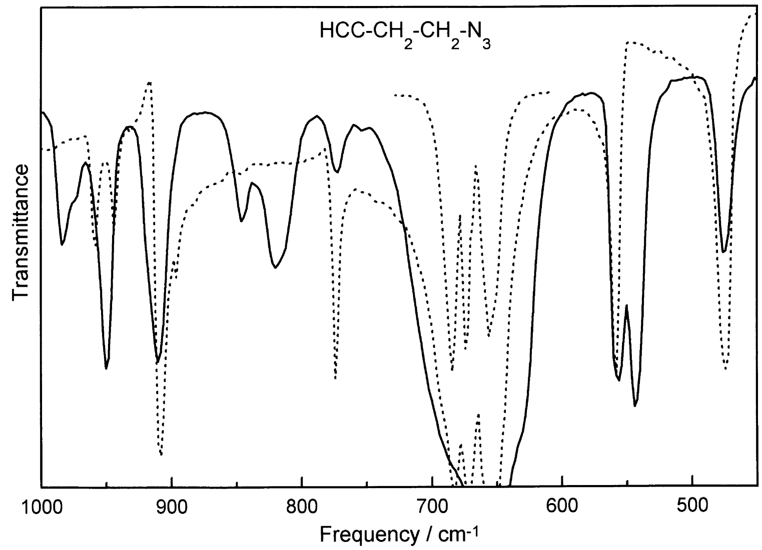

Fig. 6. Infrared spectrum of BUTAZ as an amorphous (solid line) and a crystalline solid (dotted line) at 80 K in the region 1000–450 cm$^{-1}$.

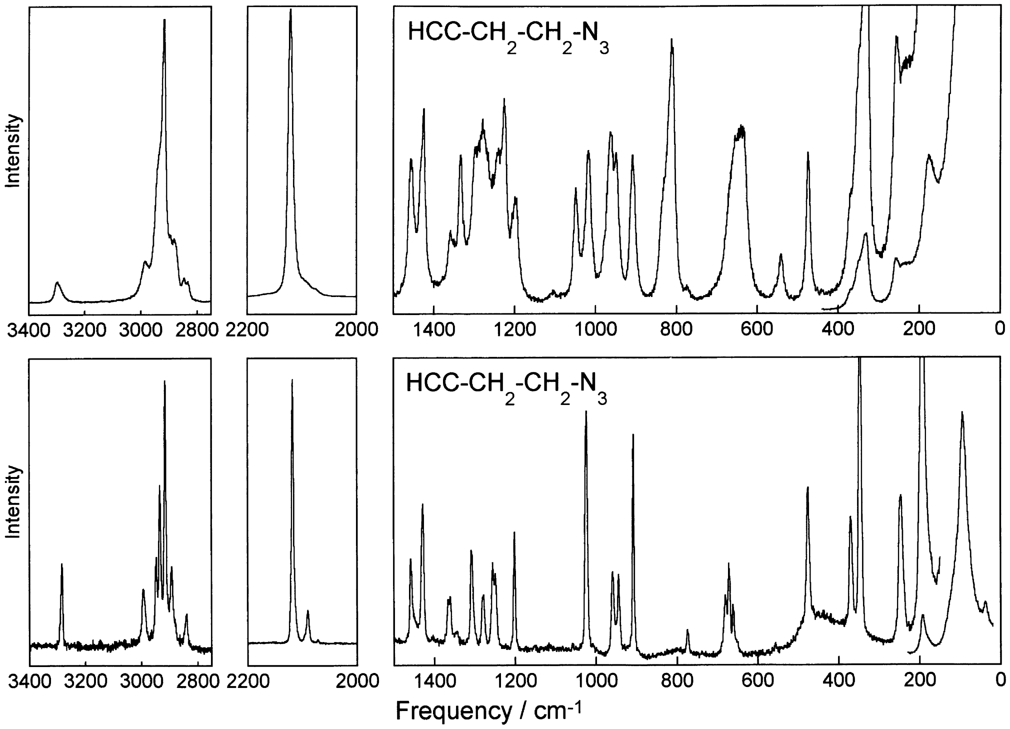

Fig. 7. Raman spectrum of BUTAZ as a liquid at 295 K (top) and as a crystalline solid (bottom) at 148 K.

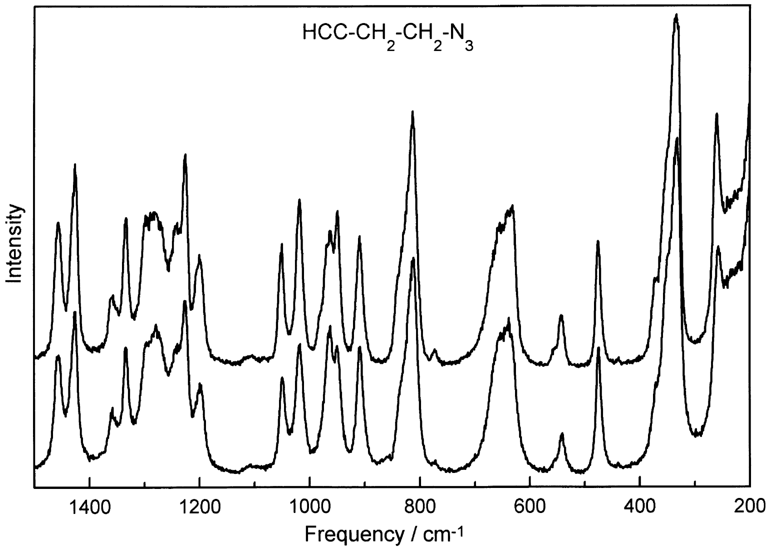

Fig. 8. Raman spectrum of BUTAZ as a liquid at 232 K (upper line) and at 293 K (lower line).

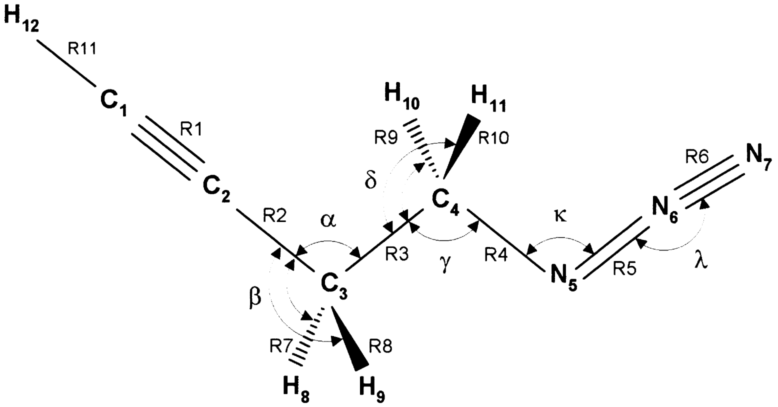

Fig. 9. Internal co-ordinates and atomic numbering in 4-azidobut-1-yne.

the Raman spectra obtained at different temperatures. In the 1300–750 cm$^{-1}$ region certain bands, e.g. at 1280, 1241, 977, 968, 964 cm$^{-1}$, are enhanced with increasing temperature, but due to extensive overlap of bands from different conformers the striving was unsuccessful. In the low frequency region the Raman bands at 349 and 252 cm$^{-1}$ are clearly enhanced with temperature, but attempts to analyse their intensity variation relative to neighbouring bands were futile.

In the 600–400 cm$^{-1}$ region there are only a few bands in the Raman spectra. The 476 cm$^{-1}$ band is well resolved; it increases the intensity relative to the band at 542 cm$^{-1}$ (Fig. 8) and remains in the spectra after crystallisation (Fig. 7). The 542 cm$^{-1}$ band slightly overlaps the very weak band at 556 cm$^{-1}$, but it definitely disappears after crystallisation. This means that the two main bands in this region, 476 and 542 cm$^{-1}$, belong to different conformers. The temperature variation of this band pair was analysed according to the van't Hoff equation indicating an enthalpy difference of 3 ± 1 kJ mol$^{-1}$ (±3σ).

### 3.2. Crystal spectra

The infrared spectra of the crystal were obtained by annealing the amorphous phase from liquid nitrogen temperature going close to the melting point, whereas the Raman crystal spectra were obtained by cooling the liquid below the melting point. The observed low temperature spectra are in both cases similar (Figs. 5–7), indicating that the same crystal phase was formed. The disappearance of several strong bands can be seen by comparing with the infrared spectra of the amorphous solid and in particular with the liquid phase Raman spectra. The vast majority of these bands do not increase their relative intensities with increasing temperature (see above). It can therefore be established that BUTAZ, like 3-azidopropene [1,2], crystallises in a conformation that is different from the low energy rotamer in the liquid.

### 3.3. Matrix spectra

Matrix isolation in combination with the hot nozzle technique offers another possibility to distinguish bands from the less stable conformers. However, the IR spectra both in the nitrogen and the argon matrices obtained with nozzle temperatures of 313 and 600 K are very similar. Some weak bands at 313 K which could belong to the less stable conformers are even weaker at 600 K. From this we draw the conclusion that the barriers between the less and more stable conformers are low and that an interconversion process probably has occurred during deposition. Judging from the matrix temperature of 12–14 K, the barrier must be around 5–6 kJ mol$^{-1}$. We are therefore not able to estimate the energy difference between the conformers from the matrix spectra. The spectra of the nitrogen matrices contain fewer bands than the argon matrices and some weak bands are missing (Fig. 3). This has been interpreted in terms of slightly lower barriers between the conformers in the nitrogen than in the argon matrices. Hence, not all conformers present in the argon are trapped in the nitrogen matrix, as was also observed for 3-azidopropene [1,2].

Following our results on 3-azidopropene [1,2], we also expect a higher barrier around the C–C bond than around the C–N bond in BUTAZ. Therefore, the BUTAZ conformers can be divided into two groups according to the conformation around the C–C bond: the *gauche* conformers (GG, GG′, GA) and the *anti* conformers (AG, AA). Interconversion processes between the conformers are more readily achieved within each group, involving merely rotations around the C–N bond with low barriers. A slower conversion is expected between the conformers from different groups where rotation with a higher barrier around the C–C bond is required. After applying the ‘mild’ and ‘strong’ annealing process (see Section 2) to the argon and nitrogen matrices four groups of bands could be distinguished:

(a) Bands which increase their relative intensity after both annealing processes (lowest energy conformer in the matrices—conformer I).
(b) Bands which do not change their relative intensity after mild annealing, but after strong annealing they definitely decrease their relative intensity and which correspond to the bands present in the crystal (the second most stable conformer—conformer II).
(c) Bands which after mild annealing decrease their relative intensity and after strong annealing practically disappear (third most stable conformer—conformer III).
(d) Bands which practically disappear upon mild annealing (highest energy conformers—conformers IV and V).

### 3.4. Ab initio calculations and normal co-ordinate analysis

Standard molecular orbital ab initio calculations were carried out for all the five BUTAZ conformers using the GAUSSIAN94 package [13]. Fully optimised geometries and vibrational spectra were calculated at the MP2(full)/TZ2P//MP2(full)/TZ2P [14–16] level of theory using standard Huzinaga TZ2P basis sets [17,18]. The optimised geometries were characterised by the Hessian matrix as true energy minima. The ab initio structure parameters of all five BUTAZ conformers are given in Table 2 and compared with the experimental data from resembling compounds. In earlier ab initio calculations with DZ basis sets [19], the C–N and N=N distances were calculated about 4 and 2 pm longer and the N≡N distance about 2 pm shorter compared to the experimental data. In a recent ab initio study of 3-azidopropene [20] at the HF-SCF level with the TZP basis set, the C–N distance was calculated to lie in the experimental range presented in Table 2. However, the N=N and N≡N distances were calculated about 1 and 4.6 pm shorter, respectively, than the experimental values. It can be seen from Table 2 that, after including the electron correlation in the geometry optimisation, the calculated C–N and N=N bond distances are both calculated near the experimental values and that the N≡N bond distance is only slightly too long. Also, the calculated bond angles and dihedral angles are calculated near the experimental values.

The ab initio energies at the MP2(full)/TZ2P//MP2(full)/TZ2P level are given in Table 3 for the five BUTAZ conformers together with SCF energies, MP2 corrections and zero-point vibration energies, ZPE. Additional single-point calculations were performed for all BUTAZ conformers at the higher MP4SDQ/TZ2P//MP2(full)/TZ2P level [21] to obtain more precise relative energies without optimising the geometry. The following relative energies (without ZPE) in kJ mol$^{-1}$ were obtained: AA, 0.00; GG, +0.37; AG, +0.61; GA, +2.84; GG′, +3.60.

From these calculations it appears that the BUTAZ conformers can be divided into two groups according to the energy: the low energy conformers, GG, AG, AA; and the high-energy conformers, GG′, GA. Recently, we have calculated the ab initio energies of all the five conformers of 3-azidopropene at the MP2/TZP//HF/TZP level [20], and the experimental conformational energies obtained were quite well reproduced. We therefore consider the calculated energies for BUTAZ at the higher level of theory as reasonably accurate. The three low energy conformers are so close in energy (Table 3) that it is difficult or impossible to settle which conformer is the most stable without additional evidence.

The ab initio calculated wavenumbers at the SCF level are usually 10–20% higher than the experimental values due to the neglect of electron correlation. At the MP2 level the calculated wavenumbers

Table 2
The ab initio calculated structural parameters of the five 4-azidobut-1-yne conformers at MP2(full)/TZ2P//MP2(full)TZ2P level. (Bond lengths in pm, bond and torsion angles in °)

| Name[a] | Internal coordinate[b] | Conformer | | | | | Experimental[c] |
|---|---|---|---|---|---|---|---|
| | | GG | GG′ | GA | AG | AA | |
| R1 | $r(C_1≡C_2)$ | 121.12 | 121.06 | 121.08 | 121.10 | 121.09 | 120.8–121.6 |
| R2 | $r(C_2–C_3)$ | 145.95 | 145.92 | 145.97 | 145.92 | 145.95 | |
| R3 | $r(C_3–C_4)$ | 153.15 | 153.16 | 152.43 | 153.30 | 152.46 | |
| R4 | $r(C_4–N_5)$ | 147.46 | 147.62 | 147.73 | 147.79 | 147.99 | 146.4–147.6 |
| R5 | $r(N_5=N_6)$ | 123.72 | 123.59 | 123.54 | 123.68 | 123.61 | 123.6–124.9 |
| R6 | $r(N_6≡N_7)$ | 114.75 | 114.89 | 114.83 | 114.86 | 114.81 | 113.2–113.8 |
| R7 | $r(C_3–H_8)$ | 108.96 | 108.93 | 108.88 | 108.94 | 108.77 | 109–111 |
| R8 | $r(C_3–H_9)$ | 108.79 | 109.00 | 108.82 | 108.78 | 108.77 | 109–111 |
| R9 | $r(C_4–H_{10})$ | 108.44 | 109.00 | 108.96 | 108.91 | 108.90 | |
| R10 | $r(C_4–C_{11})$ | 108.90 | 108.31 | 108.92 | 108.30 | 108.90 | |
| R11 | $r(C_1–H_{12})$ | 105.98 | 105.96 | 105.96 | 105.97 | 105.96 | |
| $\alpha$ | $< (C_2–C_3–C_4)$ | 111.3 | 112.1 | 111.8 | 110.4 | 110.6 | |
| $\gamma$ | $< (C_3–C_4–N_5)$ | 111.7 | 112.7 | 107.5 | 111.6 | 106.9 | 111.8–113.7 |
| $\kappa$ | $< (C_4–N_5=N_6)$ | 115.5 | 114.1 | 114.4 | 114.0 | 114.1 | 114.5–116.5 |
| $\lambda$ | $< (N_5–N_6≡N_7)$ | 172.3 | 173.4 | 173.5 | 173.4 | 173.7 | 169–174 |
| $\beta$ | $< (C_2–C_3–H_8)$ | 110.2 | 110.0 | 109.9 | 109.8 | 110.3 | 108–110 |
| $\beta$ | $< (C_2–C_3–H9)$ | 110.0 | 109.8 | 110.1 | 110.5 | 110.3 | 108–110 |
| $\delta$ | $< (C_3–C_4–H_{10})$ | 109.6 | 109.7 | 109.8 | 110.2 | 110.2 | |
| $\delta$ | $< (C_3–C_4–H_{11})$ | 110.3 | 110.4 | 110.2 | 110.2 | 110.2 | |
| t1 | $t(C_2–C_3–C_4–N_5)$ | 64.9 | 60.4 | 66.0 | 178.1 | 180.0 | |
| t2 | $t(C_3–C_4–N_5=N_6)$ | −87.5 | 61.5 | 190.4 | 69.7 | 180.0 | 60(10)[d] |
| t3 | $t(C_4–N_5–N_6≡N_7)$ | 188.1 | 181.2 | 176.4 | 178.7 | 180.0 | |
| t4 | $t(C_2–C_3–C_4–H_{10})$ | 181.5 | 183.4 | 185.5 | −58.5 | −60.0 | |
| t5 | $t(C_2–C_3–C_4–H_{11})$ | −58.8 | −56.7 | −54.3 | 61.2 | 60.0 | |

[a] Internal coordinate symbol.

[b] Numbering of the atoms according to Fig. 9.

[c] Experimental data or experimental intervals from electron diffraction data for azidoacetonitrile [3], 3-azidopropyne [4], azido-2-butyne [5] and 3-azidopropene [1,2].

[d] Dihedral angle from 3-azidopropene GG conformer (in parentheses experimental uncertainty).

are usual only about 5% too high and, therefore, just a small scaling of the force field is necessary to fit the observations. The ab initio force field calculated with the TZ2P basis set were first transformed from Cartesian co-ordinates to a set of suitable internal co-ordinates and then scaled according to the types of internal co-ordinates using the scheme: $F_{ij}(\text{scaled}) = F_{ij}(\text{ab initio})(x_i \cdot x_j)^{1/2}$, where $x_i$ and $x_j$ are scale factors for the diagonal force constants corresponding to internal co-ordinates $i$ and $j$, respectively [22].

It is our experience that the properly scaled ab initio force field represents an excellent approximation to the “real” force field, and that the predicted wavenumbers constitute a good diagnostic tool in conformational analysis [23]. For this reason six scale factors were adjusted to give the best fit between calculated wavenumbers of each individual BUTAZ conformer and the observed wavenumbers of the crystal. A common scale factor was used for force constants related to: (1) the C–H stretching co-ordinates; (2) the N≡N stretching co-ordinate; (3) the linear C≡C–C and C≡C–H bending co-ordinates; (4) the torsional co-ordinates (constrained to 1.0). Two additional scaling factors were used involving: (5) all other stretching co-ordinates and (6) all other bending co-ordinates. The results from these optimisations are summarised in Table 4. As can be seen, a good agreement with the crystal data was only achieved for the AG conformer. On this basis we conclude that the

Table 3
The ab initio energies and corresponding relative energies of 4-azidobut-1-yne conformers calculated at MP2(full)TZ2P//MP2(full)TZ2P level. (Ab initio energies in Hartree; relative energies in kJ mol$^{-1}$)

| Conformer | GG | GG′ | GA | AG | AA |
|---|---|---|---|---|---|
| $E$(SCF) | −317.676831 | −317.675677 | −317.677077 | −317.678140 | −317.679367 |
| $\Delta E$(SCF) | 6.66 | 9.67 | 6.01 | 3.22 | 0.00 |
| $E$(MP2) | −1.293620 | −1.293461 | −1.291750 | −1.291789 | −1.290257 |
| $\Delta E$(MP2) | 0.00 | 0.42 | 4.91 | 4.81 | 8.83 |
| $E$(ZPE) | 0.0888654 | 0.0888279 | 0.0886711 | 0.0888164 | 0.0886085 |
| $\Delta E$(ZPE) | 0.67 | 0.58 | 0.16 | 0.55 | 0.00 |
| $E$(SCF+MP2) | −318.970450 | −318.969138 | −318.854758 | −318.855553 | −318.855650 |
| $\Delta E$(SCF+MP2) | 0.00 | 3.44 | 4.26 | 1.37 | 2.17 |
| $E$(SCF+MP2+ZPE | −318.881585 | −318.880310 | −318.880155 | −318.881112 | −318.881015 |
| $\Delta E$(SCF+MP2+ZPE) | 0.00 | 3.35 | 3.75 | 1.24 | 1.50 |

Table 4
Comparison of the observed solid crystal and calculated vibrational frequencies of 4-azidobut-1-yne conformers. (Observed vibrational frequencies from Raman crystal spectra. Vibrational frequencies calculated with the scale factors optimised separately for each conformer on the observed solid crystal frequencies. Vibrational frequencies in cm$^{-1}$)

| No. | Obs. | Conformer | | | | | Approximate description for AG |
|---|---|---|---|---|---|---|---|
| | | GG | GG′ | GA | AG | AA | |
| $\nu_1$ | 3285 | 3294 | 3303 | 3310 | 3290 | 3301 | ≡C–H s |
| $\nu_2$ | 2995 | 2994 | 3008 | 2978 | 3006 | 2984 a″ | (N)CH$_2$ as |
| $\nu_3$ | 2948 | 2965 | 2951 | 2961 | 2960 | 2957 a″ | CH$_2$ as |
| $\nu_4$ | 2936 | 2915 | 2912 | 2930 | 2915 | 2934 | (N)CH$_2$ ss |
| $\nu_5$ | 2917 | 2915 | 2906 | 2905 | 2910 | 2907 | CH$_2$ ss |
| $\nu_6$ | 2118 | 2119 | 2168 | 2134 | 2123 | 2124 | N≡N s |
| $\nu_7$ | 2091 | 2083 | 2099 | 2099 | 2096 | 2085 | C≡C s |
| $\nu_8$ | 1459 | 1485 | 1446 | 1462 | 1484 | 1481 | (N)CH$_2$ $\delta$ |
| $\nu_9$ | 1430 | 1457 | 1422 | 1432 | 1460 | 1458 | CH$_2$ $\delta$ |
| $\nu_{10}$ | 1367 | 1360 | 1328 | 1336 | 1355 | 1354 | (N)CH$_2$ wa |
| $\nu_{11}$ | 1309 | 1343 | 1316 | 1328 | 1307 | 1290 a″ | (N)CH$_2$ tw |
| $\nu_{12}$ | 1279 | 1284 | 1272 | 1263 | 1282 | 1270 | CH$_2$ wa |
| $\nu_{13}$ | 1256 | 1227 | 1219 | 1237 | 1242 | 1246 | N=N s |
| $\nu_{14}$ | 1202 | 1214 | 1181 | 1190 | 1200 | 1186 a″ | CH$_2$ tw |
| $\nu_{15}$ | 1060 | 1058 | 1062 | 1065 | 1061 | 1059 | (N)CH$_2$ ro |
| $\nu_{16}$ | 1025 | 1015 | 1020 | 1024 | 1030 | 1049 a″ | C–C s |
| $\nu_{17}$ | 960 | 953 | 962 | 987 | 955 | 965 | ≡C–C s |
| $\nu_{18}$ | 908 | 851 | 847 | 845 | 908 | 915 | C–N s |
| $\nu_{19}$ | 775 | 811 | 827 | 827 | 774 | 776 a″ | CH$_2$ ro |
| $\nu_{20}$ | 681 | 685 | 681 | 687 | 688 | 694 | N=N≡N $\delta$ |
| $\nu_{21}$ | 672 | 679 | 671 | 675 | 675 | 680 | C≡CH $\delta$ bip |
| $\nu_{22}$ | 662 | 660 | 661 | 643 | 669 | 669 a″ | C≡CH $\delta$ bop |
| $\nu_{23}$ | 557 | 549 | 555 | 554 | 554 | 551 a″ | N=N $\tau$ |
| $\nu_{24}$ | 476 | 541 | 537 | 541 | 481 | 480 | CCC $\delta$ |
| $\nu_{25}$ | 371 | 360 | 365 | 352 | 367 | 347 a″ | CCN $\delta$ |
| $\nu_{26}$ | 349 | 340 | 331 | 325 | 342 | 336 | C≡CC $\delta$ bop |
| $\nu_{27}$ | 247 | 249 | 233 | 200 | 217 | 207 | CN=N $\delta$ |
| $\nu_{28}$ | 195 | 164 | 151 | 168 | 150 | 109 a″ | C≡CC $\delta$ bip |
| $\nu_{29}$ | 94 | 85 | 115 | 110 | 70 | 96 | C–N $\tau$ |
| $\nu_{30}$ | 40 | 68 | 36 | 32 | 68 | 53 a″ | C–C $\tau$ |

Table 5
Comparison of the calculated and experimental vibrational frequencies of 4-azidobut-1-yne conformers. (All vibrational frequencies calculated with the scale factors obtained for the AG conformer. Experimental vibrational frequencies from IR Ar-matrix spectra. Vibrational frequencies in cm$^{-1}$)

| No. | Conformer | | | | | | | | | | Approximate description for GG |
|---|---|---|---|---|---|---|---|---|---|---|---|
| | GG | | GG$'$ | | GA | | AG | | AA | | |
| | calc. | exp. | calc. | exp. | calc. | exp. | calc. | exp. | calc. | exp. | |
| $\nu_1$ | 3290 | | 3291 | | 3291 | | 3290 | 3322 | 3290 | | ≡C–H s |
| $\nu_2$ | 2988 | | 3002 | | 2963 | | 3006 | 2983 | 2973 a$''$ | | (N)CH$_2$ as |
| $\nu_3$ | 2960 | | 2945 | | 2946 | | 2960 | 2944 | 2946 a$''$ | | CH$_2$ as |
| $\nu_4$ | 2910 | | 2906 | | 2915 | | 2915 | 2938 | 2924 | | (N)CH$_2$ ss |
| $\nu_5$ | 2909 | | 2900 | | 2891 | | 2910 | 2918 | 2897 | | CH$_2$ ss |
| $\nu_6$ | 2131 | | 2127 | | 2135 | | 2123 | 2135 | 2129 | | N≡N s |
| $\nu_7$ | 2095 | | 2099 | | 2099 | | 2096 | 2106 | 2098 | | C≡C s |
| $\nu_8$ | 1478 | 1463 | 1480 | | 1481 | | 1484 | 1465 | 1487 | | (N)CH$_2$ $\delta$ |
| $\nu_9$ | 1450 | 1429 | 1455 | | 1450 | | 1460 | 1436 | 1463 | | CH$_2$ $\delta$ |
| $\nu_{10}$ | 1354 | 1361 | 1356 | 1344 | 1351 | 1338 | 1355 | 1361 | 1359 | 1352 | (N)CH$_2$ wa |
| $\nu_{11}$ | 1338 | 1336 | 1341 | | 1342 | | 1307 | 1316 | 1295 a$''$ | 1312 | CH$_2$ wa |
| $\nu_{12}$ | 1284 | 1301 | 1265 | 1309 | 1263 | 1309 | 1282 | 1276 | 1274 | 1292 | N=N s |
| $\nu_{13}$ | 1225 | 1226 | 1241 | 1255 | 1246 | 1255 | 1242 | 1269 | 1253 | 1243 | CH$_2$ tw |
| $\nu_{14}$ | 1211 | 1198 | 1200 | | 1205 | | 1200 | 1211 | 1190 a$''$ | 1181 | (N)CH$_2$ tw |
| $\nu_{15}$ | 1054 | 1059 | 1062 | | 1063 | | 1061 | 1062 | 1066 | | (N)CH$_2$ ro |
| $\nu_{16}$ | 1019 | 1018 | 1013 | | 1023 | | 1030 | 1022 | 1052 a$''$ | 1040 | C–C s |
| $\nu_{17}$ | 953 | 956 | 957 | | 986 | 972 | 955 | 977 | 971 | 989 | C–N s |
| $\nu_{18}$ | 851 | 849 | 829 | 832 | 839 | 832 | 908 | 922 | 921 | 915 | CH$_2$ ro |
| $\nu_{19}$ | 814 | 810 | 827 | 817 | 827 | 817 | 774 | 774 | 779 a$''$ | | ≡C–C s |
| $\nu_{20}$ | 676 | 656 | 675 | | 674 | | 688 | 681 | 680 | | C≡CH $\delta$ bip |
| $\nu_{21}$ | 670 | 648 | 673 | | 662 | | 675 | 672 | 671 | | C≡CH $\delta$ bop |
| $\nu_{22}$ | 657 | 634 | 662 | | 647 | | 669 | 662 | 666 a$''$ | | N=N≡N $\delta$ |
| $\nu_{23}$ | 546 | 556 | 556 | | 555 | | 554 | 556 | 551 a$''$ | | CCC $\delta$ |
| $\nu_{24}$ | 540 | 543 | 542 | | 541 | | 481 | 470 | 477 | | N=N $\tau$ |
| $\nu_{25}$ | 358 | 372 | 369 | | 351 | | 367 | 372 | 341 a$''$ | | CCN $\delta$ |
| $\nu_{26}$ | 337 | 339 | 329 | | 323 | | 342 | 348 | 337 | 334 | C≡CC $\delta$ bop |
| $\nu_{27}$ | 247 | 264 | 235 | | 199 | | 217 | 258 | 206 | | CN=N $\delta$ |
| $\nu_{28}$ | 163 | | 153 | | 169 | | 150 | 195 | 109 a$''$ | | C≡CC $\delta$ bip |
| $\nu_{29}$ | 85 | | 115 | | 110 | | 70 | 94 | 96 | | C–C $\tau$ |
| $\nu_{30}$ | 68 | | 36 | | 32 | | 68 | 40 | 53 a$''$ | | C–N $\tau$ |

conformer present in the crystal phase (conformer II) is the AG form.

The scaling factors for the AG conformer were: 0.968 for stretching, 0.958 for bending, 0.887 for C–H stretching, 0.838 for N≡N stretching and 1.120 for the linear bendings. These scale factors were subsequently employed in scaling the ab initio force fields of the other four conformers and the calculated wavenumbers are presented in Table 5. As can be seen from Table 5, there is a good correlation between the predicted wavenumbers of the GG conformer and those of group (a). The predicted wavenumbers of the AA conformer correlates best with those of group (c). Finally, some of the week bands of group (d) can be correlated with the high energy GG$'$ and GA conformers (see Section 3.3 for definition of groups).

The N=N torsion (or out-of-plane bending mode) of the azido group is largely insensitive to the molecular conformation [24]. It usually appears around 555 cm$^{-1}$ as a medium to weak band in the infrared, and as a very weak band (or even absent) in the Raman spectra. In agreement with the normal co-ordinate calculations, the medium to weak IR band at 554 cm$^{-1}$ (liquid) with its very weak Raman counterpart at 556 cm$^{-1}$ was assigned to this mode in all conformers. According to the normal co-ordinate calculations, the other two bands in this region, the

542 and 476 cm$^{-1}$ bands, originate from the C–C–C bending modes of the GG, GG′, GA conformers (C–C *gauche*), and the AG and AA conformers (C–C *anti*), respectively. Therefore, the 542 and 476 cm$^{-1}$ bands, showing a temperature variation corresponding to an enthalpy difference of 3 ± 1 kJ mol$^{-1}$, are not conformationally pure and the energy difference should be regarded as an average energy difference between several conformers. The dipole moments of the C–C *gauche* and C–C *anti* conformers are roughly 2.0 and 1.3 D [9], respectively, and the *gauche* conformers are therefore likely further stabilised in the neat liquid [25,26]. Assuming that the intensity contribution to the Raman band at 542 cm$^{-1}$ from the high-energy conformers (GG′, GA) is negligible, the estimated enthalpy difference between the GG conformer and the AG/AA conformers, 3 ± 1 kJ mol$^{-1}$, is in agreement with the theoretical value.

## 4. Conclusions

The ab initio assisted interpretation of the vibrational spectra suggests that the most stable conformation of BUTAZ in the gas phase and in the liquid is the GG form. In order of decreasing stability follows the AG and the AA forms. All these three conformers differ only slightly in energy as evident from both ab initio calculations and from the small temperature dependence of the liquid phase and the matrix isolation spectra. A few bands in the argon matrix and in the liquid phase spectra could be assigned to the less stable GG′ and GA conformers. The Raman spectra show unambiguously that the most stable conformer in the liquid (GG) is not the one present in the low temperature crystal (AG). Unfortunately, we were not able to estimate the energy differences between the GG, AG and AA conformers from the Raman spectra of the liquid as bands from the different conformers were either overlapping or poorly resolved. The barriers to rotation around the C–N bond are probably so low (around 5–6 kJ mol$^{-1}$) that conformational interconversion occurs during relaxation of the matrices at 12–14 K.

By comparison with other unsaturated azides containing the $-CH_2N_3$ moiety [1–5], it is clear that the incision of a second methylene group between the π-electron system of the multiple bond and the azido group decreases the stabilisation effect of their mutual interaction. This is reflected in the small energy difference calculated between the low and high energy conformations in BUTAZ compared with the corresponding values for azidoacetonitrile [3], 3-azidopropyne [4] and azido-2-butyne [5].

## Acknowledgements

A.G. gratefully acknowledges the “Konferenz der Deutschen Akademien der Wissenschaften” for a scholarship. This work was supported by the Slovak Grant Agency for Science project No. 1/990939/95 and by TU Brno grants No. 0006/95 and No. 0072/95. The calculations were performed on the SGI Power Challenge computers of the Supercomputer centre of the Czech Republic in Prague and Brno. The authors are also indebted to R. Konecny, University of Delaware, Newark DE, USA for valuable help with the time consuming MP4 calculations.

## References

[1] P. Klaeboe, K. Kosa, C.J. Nielsen, H. Priebe, S.H. Schei, J. Mol. Struct. 176 (1988) 107.
[2] A. Gatial, P. Klaeboe, C.J. Nielsen, H. Priebe, J. Mol. Struct. 200 (1989) 443.
[3] P. Klaeboe, K. Kosa, C.J. Nielsen, H. Priebe, S.H. Schei, J. Mol. Struct. 160 (1987) 245.
[4] J. Almlöf, G.O. Braathen, P. Klaeboe, C.J. Nielsen, H. Priebe, S.H. Schei, J. Mol. Struct. 160 (1987) 1.
[5] C.J. Nielsen, H. Priebe, R. Salzer, S.H. Schei, J. Mol. Struct. 162 (1987) 41.
[6] C.J. Nielsen, K. Kosa, H. Priebe, C.E. Sjøgren, Spectrochim. Acta 44A (1988) 409.
[7] S. Sklenák, S. Biskupic, A. Gatial, J. Mol. Struct. (Theochem) 397 (1997) 249.
[8] A. Gatial, S. Sklenák, P. Klaeboe, C.J. Nielsen, H. Priebe, R. Salzer, D. Kurková, Mol. Struct. 349 (1995) 149.
[9] S. Sklenák, S. Biskupic, A. Gatial, J. Mol. Struct. (Theochem) 336 (1995) 75.
[10] H. Priebe, Acta Chem. Scand. Part B 38 (1984) 623 see also p. 895.
[11] H.H. Günthard, J. Mol. Struct. 80 (1982) 87.
[12] F.A. Miller, B.M. Harney, Appl. Spectrosc. 28 (1968) 350.
[13] GAUSSIAN94, (Revision A1), M.J. Frisch, G.W. Trucks, H.B. Schlegel, P.M.W. Gill, B.G. Johnson, M.A. Robb, J.R. Cheeseman, T.A. Keith, G.A. Petersson, J.A. Montgomery, K. Raghavachari, M.A. Al-Laham, V.G. Zakrzewski, J.V. Ortiz, J.B. Foresman, J. Cioslowski, B.B. Stefanov, A. Nanayakkara, M. Challacombe, C.Y. Peng, P.Y. Ayala, W.

Chen, M.W. Wong, J.L. Andres, E.S. Replogle, R. Gomperts, R.L. Martin, D.J. Fox, J.S. Binkley, D.J. Defrees, J. Baker, J.J.P. Stewart, M. Head-Gordon, C. Gonzales, J.A. Pople, Gaussian, Inc., Pittsburgh, PA, 1995.
[14] M. Head-Gordon, J.A. Pople, M.J. Frisch, Chem. Phys. Lett. 153 (1988) 503.
[15] M.J. Frisch, M. Head-Gordon, J.A. Pople, Chem. Phys. Lett. 166 (1990) 275.
[16] M.J. Frisch, M. Head-Gordon, J.A. Pople, Chem. Phys. Lett. 166 (1990) 281.
[17] S. Huzinaga, J. Chem. Phys. 42 (1965) 1293.
[18] T.H. Dunning, J. Chem. Phys. 53 (1970) 2823.
[19] C.J. Nielsen, C.E. Sjøgren, J. Mol. Struct. 150 (1987) 361.
[20] A. Gatial, S. Biskupic, P. Klaeboe, C.J. Nielsen, Z. Phys. Chem. 191 (1995) 145.
[21] R. Krishnan, J.A. Pople, Int. J. Quant. Chem. 14 (1978) 91.
[22] P. Pulay, G. Fogarasi, G. Pongor, J.E. Boggs, A. Vargha, J. Am. Chem. Soc. 105 (1983) 7037.
[23] D.L. Powell, A. Gatial, P. Klaeboe, C.J. Nielsen, A.J. Kondow, J. Mol. Struct. 300 (1993) 209.
[24] P. Klaeboe, C.J. Nielsen, in: R. Salzer, H. Kriegsmann, G. Werner (Eds.), Proc. Analytiktreffen, Teubner-Texte zur Physik, Leipzig, 1988, p. 125.
[25] R.J. Abraham, E. Bretschneider, in: W.J. Orville-Thomas (Ed.), Internal Rotation in Molecules, Wiley, New York, 1974.
[26] L. Onsager, J. Am. Chem. Soc. 58 (1936) 1486.